

# FUNDAMENTAL SOLUTION BASED GRADED ELEMENT MODEL FOR STEADY-STATE HEAT TRANSFER IN FGM<sup>\*\*</sup>

Leilei Cao<sup>1,2</sup>    Hui Wang<sup>2,3</sup>    Qing-Hua Qin<sup>2\*</sup>

(<sup>1</sup>Key Laboratory for Highway Construction Technology and Equipment of Ministry of Education, Chang'an University, Xi'an 710064, China)

(<sup>2</sup>School of Engineering, Australian National University, Canberra, ACT 0200, Australia)

(<sup>3</sup>College of Civil Engineering and Architecture, Henan University of Technology, Zhengzhou 450052, China)

Received 7 May 2011, revision received 9 September 2011

**ABSTRACT** A novel hybrid graded element model is developed in this paper for investigating thermal behavior of functionally graded materials (FGMs). The model can handle a spatially varying material property field of FGMs. In the proposed approach, a new variational functional is first constructed for generating corresponding finite element model. Then, a graded element is formulated based on two sets of independent temperature fields. One is known as intra-element temperature field defined within the element domain; the other is the so-called frame field defined on the element boundary only. The intra-element temperature field is constructed using the linear combination of fundamental solutions, while the independent frame field is separately used as the boundary interpolation functions of the element to ensure the field continuity over the inter-element boundary. Due to the properties of fundamental solutions, the domain integrals appearing in the variational functional can be converted into boundary integrals which can significantly simplify the calculation of generalized element stiffness matrix. The proposed model can simulate the graded material properties naturally due to the use of the graded element in the finite element (FE) model. Moreover, it inherits all the advantages of the hybrid Trefftz finite element method (HT-FEM) over the conventional FEM and boundary element method (BEM). Finally, several examples are presented to assess the performance of the proposed method, and the obtained numerical results show a good numerical accuracy.

**KEY WORDS** graded element, hybrid FEM, heat conduction, functionally graded materials

## I. INTRODUCTION

FGMs are a class of relatively new and promising composite materials that have optimized material properties by combining different material components following a predetermined law. The gradual change in terms of special variables offers a gradient of properties and performances<sup>[1]</sup>. For instance, a material that transitions smoothly from a pure metal to a pure ceramic would integrate the advantages of the two components (metal and ceramic here). It is noted that functionally graded materials are frequently used in structures under thermal load, and it is, therefore, necessary to develop some effective numerical methods for analyzing thermal properties of FGMs.

---

\* Corresponding authors. E-mail: qinghua.qin@anu.edu.au

\*\* The research in this paper is partially supported by the Special Fund for Basic Scientific Research of Central Colleges, Chang'an University (Project No. CHD2011JC150) and the National Natural Science Foundation of China (No. 11102059).

In general, the thermal conductivity of FGMs varies continuously in one or two spatial directions, so the exact solution of FGMs is usually difficult to obtain, except for some simple cases. To obtain solutions for FGMs with complex geometry and loading conditions, various numerical algorithms have been developed during the past decades. For example, finite element method (FEM)<sup>[2,3]</sup>, the boundary element method (BEM)<sup>[4,5]</sup> or dual reciprocity BEM<sup>[6,7]</sup> have been used to analyze the static or dynamic thermal response of FGMs. Additionally, some meshless or meshfree approaches, such as the meshless local Petrov-Galerkin (MLPG) method<sup>[8]</sup>, the meshless local boundary integral equation (LBIE) method<sup>[9]</sup> and the method of fundamental solution (MFS)<sup>[10-14]</sup> have also been developed for solving heat conduction problems in both isotropic and anisotropic, single and multi-materials, as well as linear and nonlinear FGMs. In particular, the following two models have been developed specially for FGMs. The first one is the conventional homogeneous elements model<sup>[15,16]</sup>, in which the element rows are aligned with the gradient direction and the property of each row of the homogeneous elements is taken to be the property at the centroid of the element and the material gradient is achieved by constructing a highly refined mesh. This produces a stepwise constant approximation to a continuous material property field. The second one is the graded finite element model<sup>[2,17,18]</sup>, in which the material gradient is directly sampled by assigning corresponding material properties at the Gauss integration points.

In this paper, a hybrid graded element model is developed for analyzing two-dimensional heat conduction problems in both isotropic and anisotropic graded materials. This study builds upon the hybrid finite element formulation with fundamental solutions as internal interpolation functions (HFS-FEM) proposed by Wang and Qin<sup>[19]</sup> and presents a special graded element for FGMs. The HFS-FEM inherits the advantages of the hybrid Trefftz finite element method (HT-FEM)<sup>[20,21]</sup> over the conventional FEM and boundary element method (BEM), and removes the difficulty in deriving and selecting appropriate terms of T-complete functions used in HT-FEM, as the fundamental solution is relatively easy to be constructed (or can be found for most physical problems in the literature) and contains usually one term only, rather than a series containing infinite terms for T-complete functions. In the analysis, a linear combination of the fundamental solution for functionally graded materials at different source points is used to approximate the field variable within the element and an independent frame field defined along the element boundary is employed to guarantee the inter-element continuity. A variational functional is constructed to generate the final stiffness equation and establish the link between the boundary frame field and internal field within an element. The proposed graded element formulation can incorporate the graded material property at the size of element level, so it is more natural than conventional homogeneous elements model and Gauss point sampling model discussed above<sup>[15,17]</sup>. Besides, other hybrid approaches for developing high performance finite element models can be found in Refs.[22,23] by introducing Airy stress functions in the complementary energy functional.

The paper begins with a brief description of heat conduction problems in FGMs in §II. Then, a detailed derivation of the proposed HFS-FEM with graded element and the corresponding algorithm is described in §III to provide an initial insight on this new finite element model. Several numerical examples for both isotropic and anisotropic cases are presented in §IV to assess the proposed algorithm and some concluding remarks are presented in §V.

## II. STATEMENT OF HEAT CONDUCTION PROBLEMS IN FGM

### 2.1. Basic Formulations

Consider a 2D steady-state heat conduction problem defined in an anisotropic inhomogeneous media without internal heat sources:

$$(\tilde{K}_{ij}(\mathbf{X})u_{,j})_{,i} = 0 \quad \forall \mathbf{X} \in \Omega \quad (1)$$

with following boundary conditions:

—Specified temperature boundary condition

$$u = \bar{u} \quad \text{on } \Gamma_u \quad (2)$$

—Specified heat flux boundary condition

$$q = -\tilde{K}_{ij}u_{,j}n_i = \bar{q} \quad \text{on } \Gamma_q \quad (3)$$

—Convection boundary condition

$$q = h(u - u_\infty) \quad \text{on } \Gamma_c \quad (4)$$

where  $\tilde{K}_{ij}$  denotes the thermal conductivity in terms of spatial variable  $\mathbf{X}$  and is assumed to be symmetric and positive-definite ( $\tilde{K}_{12} = \tilde{K}_{21}$ ,  $\det \tilde{K} = \tilde{K}_{11}\tilde{K}_{22} - \tilde{K}_{12}^2 > 0$ ).  $u$  is the sought field variable and  $q$  represents the boundary heat flux.  $n_j$  is the direction cosine of the unit outward normal vector  $\mathbf{n}$  to the boundary  $\Gamma = \Gamma_u \cup \Gamma_q \cup \Gamma_c$ , and  $\bar{u}$  and  $\bar{q}$  are specified functions on the related boundaries, respectively.  $h$  is the coefficient of heat convection, and  $u_\infty$  is the ambient environment temperature. For convenience, the space derivatives are indicated by a comma, i.e.  $u_{,j} = \partial u / \partial X_j$ , and the subscript index  $i, j$  takes values 1 and 2 in our analysis. Moreover, repeated subscript indices stand for summation convention.

## 2.2. Fundamental Solution in FGMs

For simplicity, we assume the thermal conductivity varies exponentially with position vector, for example

$$\tilde{K}(\mathbf{X}) = \mathbf{K} \exp(2\boldsymbol{\beta} \cdot \mathbf{X}) \quad (5)$$

where vector  $\boldsymbol{\beta} = (\beta_1, \beta_2)$  is a graded parameter and matrix  $\mathbf{K}$  is symmetric and positive-definite with constant entries.

Substituting Eq.(5) into Eq.(1) yields

$$K_{ij}u_{,ij}(\mathbf{X}) + 2\beta_i K_{ij}u_{,j}(\mathbf{X}) = 0 \quad (6)$$

whose fundamental function defined in the infinite domain must satisfy the following equation:

$$K_{ij}N_{,ij}(\mathbf{X}, \mathbf{X}_s) + 2\beta_i K_{ij}N_{,j}(\mathbf{X}, \mathbf{X}_s) + \delta(\mathbf{X}, \mathbf{X}_s) = 0 \quad (7)$$

in which  $\mathbf{X}$  and  $\mathbf{X}_s$  denote arbitrary field point and source point in the infinite domain, respectively.  $\delta$  is the Dirac delta function.

The closed-form solution to Eq.(6) in two dimensions can be expressed as<sup>[24]</sup>

$$N(\mathbf{X}, \mathbf{X}_s) = -\frac{K_0(\kappa R)}{2\pi\sqrt{\det \mathbf{K}}} \exp\{-\boldsymbol{\beta} \cdot (\mathbf{X} + \mathbf{X}_s)\} \quad (8)$$

where  $\kappa = \sqrt{\boldsymbol{\beta} \cdot \mathbf{K} \boldsymbol{\beta}}$ ,  $R$  is the geodesic distance defined as  $R = R(\mathbf{X}, \mathbf{X}_s) = \sqrt{\mathbf{r} \cdot \mathbf{K}^{-1} \mathbf{r}}$  and  $\mathbf{r} = \mathbf{r}(\mathbf{X}, \mathbf{X}_s) = \mathbf{X} - \mathbf{X}_s$ .  $K_0$  is the modified Bessel function of the second kind of zero order. For isotropic materials,  $K_{12} = K_{21} = 0$ ,  $K_{11} = K_{22} = k_0 > 0$ , Eq.(6) recasts as

$$k_0 \nabla^2 u(\mathbf{X}) + 2k_0 \beta_i u_{,i}(\mathbf{X}) = 0 \quad (9)$$

Then the fundamental solution given by Eq.(8) reduces to

$$N(\mathbf{X}, \mathbf{X}_s) = -\frac{K_0(\kappa R)}{2\pi k_0} \exp[-\boldsymbol{\beta} \cdot (\mathbf{X} + \mathbf{X}_s)] \quad (10)$$

which agrees with the result in Ref.[25].

## III. GENERATION OF GRADED ELEMENT

In this section, the procedure for developing a hybrid graded element model is described based on the boundary value problem (BVP) defined in Eqs.(1)-(3). The focus is to fully introduce the smooth variation of material properties into element formulation, instead of stepwise constant approximation frequently used in the conventional FEM.

Similar to HT-FEM, the main idea of the proposed approach is to establish an appropriate hybrid FE formulation whereby intra-element continuity is enforced on a nonconforming internal displacement field formed by a linear combination of fundamental solutions at points outside the element domain under consideration, while an auxiliary frame field is independently defined on the element boundary to enforce the field continuity across inter-element boundaries. But unlike in the HT-FEM, the

intra-element fields are constructed based on the fundamental solution defined in Eq.(7), rather than T-functions. Consequently, a variational functional corresponding to the new trial function is required to derive the related generalized stiffness matrix equation. With the problem domain divided into some sub-domains or elements denoted by  $\Omega_e$  with the element boundary  $\Gamma_e$ , additional continuities are usually required on the common boundary  $\Gamma_{Ief}$  between any two adjacent elements ‘e’ and ‘f’ (see Fig.1):

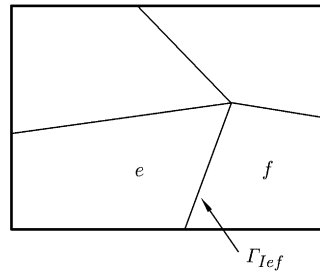


Fig. 1 Illustration of continuity between two adjacent elements ‘e’ and ‘f’.

$$\left. \begin{aligned} u_e &= u_f && \text{(conformity)} \\ q_e + q_f &= 0 && \text{(reciprocity)} \end{aligned} \right\} \text{ on } \Gamma_{Ief} = \Gamma_e \cap \Gamma_f \tag{11}$$

in the proposed hybrid FE approach.

**3.1. Non-conforming Intra-element Field**

The idea of method of fundamental solution (MFS)<sup>[26]</sup> is adopted here to remove the singularity of fundamental solution. For a particular element, say element *e*, which occupies sub-domain  $\Omega_e$ , we first assume that the field variable within an element is extracted from a linear combination of fundamental solutions centered at different source points (see Fig.2), that is,

$$u_e(\mathbf{x}) = \sum_{j=1}^{n_s} N_e(\mathbf{x}, \mathbf{x}_{sj}) c_{ej} = \mathbf{N}_e(\mathbf{x}) \mathbf{c}_e \quad \forall \mathbf{x} \in \Omega_e, \mathbf{x}_{sj} \notin \Omega_e \tag{12}$$

where  $c_{ej}$  is undetermined coefficients and  $n_s$  is the number of virtual sources outside the element *e*.  $N_e$  is the required fundamental solution expressed in local element coordinates  $(x_1, x_2)$ , instead of global coordinates  $(X_1, X_2)$ (see Fig.2).

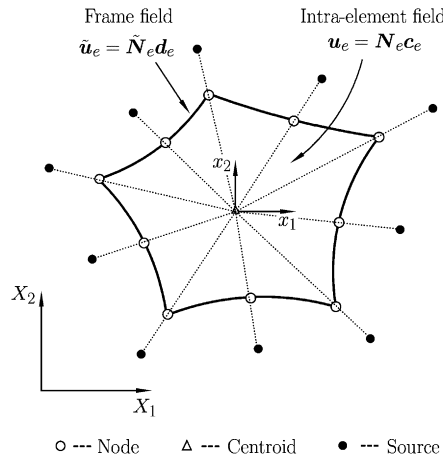


Fig. 2. Intra-element field, frame field in a particular element, and generation of source points in HFS-FEM.

Evidently, Eq.(12) analytically satisfies the heat conduction equation (6) due to the inherent property of  $N_e(\mathbf{x}, \mathbf{x}_{sj})$ .

In practice, the generation of virtual source points is usually done by means of the following formulation employed in the meshless method<sup>[27]</sup>:

$$\mathbf{x}_{sj} = \mathbf{x}_{bj} + \gamma(\mathbf{x}_{bj} - \mathbf{x}_c) \tag{13}$$

where  $\gamma$  is a dimensionless coefficient,  $\mathbf{x}_{bj}$  is a elementary boundary point and  $\mathbf{x}_c$  is the geometrical centroid of the element. For a particular element shown in Fig.2, we can use the nodes of element

to generate related source points for simplification. Either too big or too small distance between the virtue source points and physical element boundaries will affect the results due to the singularity of the fundamental solution and the restriction of computer precision including round-off error<sup>[13]</sup>.

The corresponding normal heat flux on  $\Gamma_e$  is given by

$$q_e = -\tilde{K}_{ij}u_{e,j}n_i = \mathbf{Q}_e \mathbf{c}_e \tag{14}$$

where

$$\mathbf{Q}_e = -\tilde{K}_{ij}\mathbf{N}_{e,j}n_i = \mathbf{A}\mathbf{T}_e \tag{15}$$

with

$$\mathbf{T}_e = \left[ -\left(\tilde{K}_{11}\mathbf{N}_{e,1} + \tilde{K}_{12}\mathbf{N}_{e,2}\right) \quad -\left(\tilde{K}_{21}\mathbf{N}_{e,1} + \tilde{K}_{22}\mathbf{N}_{e,2}\right) \right]^T, \quad \mathbf{A} = \{n_1 \ n_2\} \tag{16}$$

### 3.2. Auxiliary Conforming Frame Field

In order to enforce the conformity on the field variable  $u$ , for instance,  $u_e = u_f$  on  $\Gamma_e \cap \Gamma_f$  of any two neighboring elements  $e$  and  $f$ , an auxiliary inter-element frame field  $\tilde{u}$  is used and expressed in terms of the same nodal degrees of freedom (DOF)  $\mathbf{d}_e$ , as used in the conventional finite elements. In this case,  $\tilde{u}$  is confined to the whole element boundary

$$\tilde{u}_e(\mathbf{x}) = \tilde{\mathbf{N}}_e(\mathbf{x}) \mathbf{d}_e \tag{17}$$

which is independently assumed along the element boundary in terms of nodal DOF  $\mathbf{d}_e$ , where  $\tilde{\mathbf{N}}_e$  represents the conventional FE interpolating functions. For example, a simple interpolation of the frame field on a side with three nodes of a particular element can be given in the form

$$\tilde{u} = \tilde{N}_1 u_1 + \tilde{N}_2 u_2 + \tilde{N}_3 u_3 \tag{18}$$

where  $\tilde{N}_i$  ( $i = 1, 2, 3$ ) stands for shape functions in terms of natural coordinate  $\xi$  defined in Fig.3.

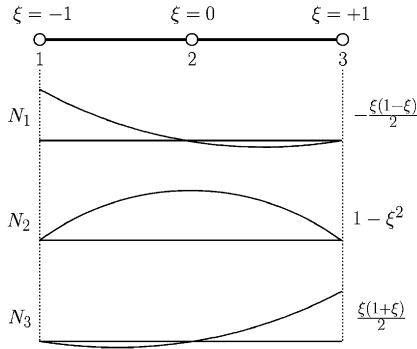


Fig. 3. Typical quadratic interpolation for the frame field.

### 3.3. Graded Element

The fundamental solution for FGM is used as  $N_e$  in Eq.(12) to approximate the intra-element field. It can be seen from Eq.(8) that  $N_e$  varied throughout each element due to different geodesic distance for each field point, so the smooth variation of material properties can be achieved by this inherent property, instead of stepwise constant approximation frequently used in the conventional FEM<sup>[4]</sup>. For example, Fig.4 illustrates the two models when the thermal conductivity varies along direction  $X_2$  in isotropic material.

It should be mentioned here that Eq.(5) which describes variation of the thermal conductivity is defined under global coordinate system. When contriving the intra-element field for each element, this formulation has to be transferred into local element coordinate defined at the center of the element, the graded matrix  $\tilde{\mathbf{K}}$  in Eq.(5) can, then, be expressed by

$$\tilde{\mathbf{K}}_e(\mathbf{x}) = \mathbf{K}_C \exp(2\boldsymbol{\beta} \cdot \mathbf{x}) \tag{19}$$

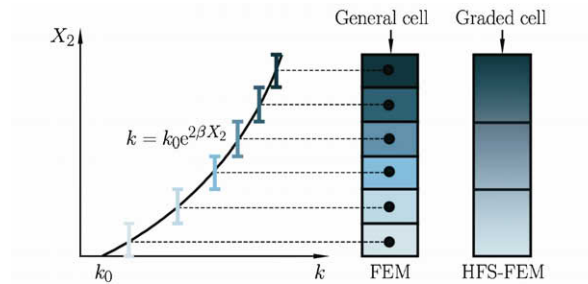


Fig. 4. Comparison of computational cell in the stepwise constant FEM and the proposed HFS-FEM.

for a particular element  $e$ , where  $\mathbf{K}_C$  denotes the value of the conductivity at the centroid of each element and can be calculated as follow:

$$\mathbf{K}_C = \mathbf{K} \exp(2\boldsymbol{\beta} \cdot \mathbf{X}_c) \quad (20)$$

where  $\mathbf{X}_c$  is the global coordinate of the element centroid.

Accordingly, the matrix  $\mathbf{K}_C$  is used to replace  $\mathbf{K}$  (see Eq.(7) ) in the formulation of fundamental solution for FGM and the construction of intra-element field under local element coordinate for each element.

### 3.4. Modified Variational Principle and Stiffness Equation

#### 3.4.1. Modified functional

For the boundary value problem defined in Eqs.(1)-(3) and (4), since the stationary conditions of the traditional potential or complementary variational functional can't guarantee the satisfaction of inter-element continuity condition required in the proposed HFS-FE model, a modified potential functional is developed as follows<sup>[19]</sup>:

$$\Pi_m = \sum_e \Pi_{me} = \sum_e \left\{ - \int_{\Omega_e} \frac{1}{2} \tilde{K}_{ij} u_{,j} u_{,i} d\Omega - \int_{\Gamma_{qe}} \bar{q} \tilde{u} d\Gamma + \int_{\Gamma_e} (\tilde{u} - u) q d\Gamma - \int_{\Gamma_{ce}} \frac{h}{2} (\tilde{u} - u_\infty)^2 d\Gamma \right\} \quad (21)$$

in which the governing equation (1) is assumed to be satisfied, *a priori*, in deriving the HFS-FE model. The boundary  $\Gamma_e$  of a particular element consists of the following parts:

$$\Gamma_e = \Gamma_{ue} \cup \Gamma_{qe} \cup \Gamma_{ce} \cup \Gamma_{Ie} \quad (22)$$

where  $\Gamma_{Ie}$  represents the inter-element boundary of the element 'e' shown in Fig.1.

The stationary condition of the functional (21) can lead to the governing equation (Euler equation), boundary conditions and continuity conditions, which is briefly shown here. Equation (21) gives the following functional defined in a particular element:

$$\Pi_{me} = -\frac{1}{2} \int_{\Omega_e} \tilde{K}_{ij} u_{,j} u_{,i} d\Omega - \int_{\Gamma_{qe}} \bar{q} \tilde{u} d\Gamma + \int_{\Gamma_e} q (\tilde{u} - u) d\Gamma - \frac{1}{2} \int_{\Gamma_{ce}} h (\tilde{u} - u_\infty)^2 d\Gamma \quad (23)$$

whose first-order variational yields

$$\begin{aligned} \delta \Pi_{me} = & - \int_{\Omega_e} \tilde{K}_{ij} u_{,j} \delta u_{,i} d\Omega - \int_{\Gamma_{qe}} \bar{q} \delta \tilde{u} d\Gamma + \int_{\Gamma_e} (\delta \tilde{u} - \delta u) q d\Gamma \\ & + \int_{\Gamma_e} (\tilde{u} - u) \delta q d\Gamma - \int_{\Gamma_{ce}} h (u - u_\infty) \delta \tilde{u} d\Gamma \end{aligned} \quad (24)$$

From the notation  $q = -\tilde{K}_{ij} u_{,j} n_i = \bar{q}$  and the Gauss theorem

$$\int_{\Omega} h_{,i} d\Omega = \int_{\Gamma} h n_i d\Gamma \quad (25)$$

for any smooth function  $h$  in the domain, we have

$$\begin{aligned} \delta \Pi_{me} = & \int_{\Omega_e} (\tilde{K}_{ij} u_{,j})_{,i} \delta u d\Omega + \int_{\Gamma_{qe}} (q - \bar{q}) \delta \tilde{u} d\Gamma + \int_{\Gamma_{ue}} q \delta \tilde{u} d\Gamma + \int_{\Gamma_{Ie}} q \delta \tilde{u} d\Gamma \\ & + \int_{\Gamma_e} (\tilde{u} - u) \delta q d\Gamma + \int_{\Gamma_{ce}} [q - h (\tilde{u} - u_\infty)] \delta \tilde{u} d\Gamma \end{aligned} \quad (26)$$

For the displacement-based method, the potential conformity should be satisfied in advance, that is,

$$\begin{aligned} \delta \tilde{u} &= 0 && \text{on } \Gamma_{ue} \text{ because } (\tilde{u} = \bar{u}) \\ \delta \tilde{u}^e &= \delta \tilde{u}^f && \text{on } \Gamma_{Ie}^f \text{ because } (\tilde{u}^e = \tilde{u}^f) \end{aligned} \quad (27)$$

then, Eq.(26) can be rewritten as

$$\begin{aligned} \delta II_{me} = & \int_{\Omega_e} (\tilde{K}_{ij}u_{,j})_{,i} \delta u d\Omega + \int_{\Gamma_{qe}} (q - \bar{q}) \delta \tilde{u} d\Gamma + \int_{\Gamma_e} q \delta \tilde{u} d\Gamma \\ & + \int_{\Gamma_e} (\tilde{u} - u) \delta q d\Gamma + \int_{\Gamma_{ce}} [q - h(\tilde{u} - u_\infty)] \delta \tilde{u} d\Gamma \end{aligned} \quad (28)$$

from which the Euler equation in the domain  $\Omega_e$ , heat flux and convection boundary conditions on  $\Gamma_e$ , and the equality of  $u$  and  $\tilde{u}$  along the element frame  $\Gamma_e$  can be obtained using the stationary condition  $\delta II_{me} = 0$ , i.e.,

$$\begin{aligned} (\tilde{K}_{ij}u_{,j})_{,i} &= 0 && \text{in } \Omega_e \\ q &= \bar{q} && \text{on } \Gamma_{qe} \\ q &= h(\tilde{u} - u_\infty) && \text{on } \Gamma_{ce} \\ \tilde{u} &= u && \text{on } \Gamma_e \end{aligned} \quad (29)$$

### 3.4.2. Stiffness equation

Having independently defined the intra-element field and frame field in a particular element (see Fig.2), we next generate the element stiffness equation through a variational approach.

The variational functional  $\Pi_e$  corresponding to a particular element  $e$  of the present problem can be written as

$$\Pi_{me} = -\frac{1}{2} \int_{\Omega_e} \tilde{K}_{ij}u_{,j}u_{,i} d\Omega - \int_{\Gamma_{qe}} \bar{q}\tilde{u} d\Gamma + \int_{\Gamma_e} q(\tilde{u} - u) d\Gamma - \int_{\Gamma_{ce}} \frac{h}{2} (\tilde{u} - u_\infty)^2 d\Gamma \quad (30)$$

Applying the Gauss theorem (25) again to the above functional, we get the following functional for the HFS-FE model:

$$\Pi_{me} = \frac{1}{2} \left[ \int_{\Gamma_e} qu d\Gamma + \int_{\Omega_e} u(\tilde{K}_{ij}u_{,j})_{,i} d\Omega \right] - \int_{\Gamma_{qe}} \bar{q}\tilde{u} d\Gamma + \int_{\Gamma_e} q(\tilde{u} - u) d\Gamma - \int_{\Gamma_{ce}} \frac{h}{2} (\tilde{u} - u_\infty)^2 d\Gamma \quad (31)$$

Considering the governing equation (1), we finally obtain the functional defined on the element boundary only

$$\Pi_{me} = -\frac{1}{2} \int_{\Gamma_e} qu d\Gamma - \int_{\Gamma_{qe}} \bar{q}\tilde{u} d\Gamma + \int_{\Gamma_e} q\tilde{u} d\Gamma - \int_{\Gamma_{ce}} \frac{h}{2} (\tilde{u} - u_\infty)^2 d\Gamma \quad (32)$$

which leads to Eq.(33) by substituting Eqs.(12), (14) and (17) into the functional (32):

$$\Pi_e = -\frac{1}{2} \mathbf{c}_e^T \mathbf{H}_e \mathbf{c}_e - \mathbf{d}_e^T \mathbf{g}_e + \mathbf{c}_e^T \mathbf{G}_e \mathbf{d}_e - \frac{1}{2} \mathbf{d}_e^T \mathbf{F}_e \mathbf{d}_e + \mathbf{d}_e^T \mathbf{f}_e - a_e \quad (33)$$

with

$$\begin{aligned} \mathbf{H}_e &= \int_{\Gamma_e} \mathbf{Q}_e^T \mathbf{N}_e d\Gamma, & \mathbf{G}_e &= \int_{\Gamma_e} \mathbf{Q}_e^T \tilde{\mathbf{N}}_e d\Gamma, & \mathbf{g}_e &= \int_{\Gamma_{qe}} \tilde{\mathbf{N}}_e^T \bar{q} d\Gamma \\ \mathbf{F}_e &= \int_{\Gamma_{ce}} h \tilde{\mathbf{N}}_e^T \tilde{\mathbf{N}}_e d\Gamma, & \mathbf{f}_e &= \int_{\Gamma_{ce}} h u_\infty \tilde{\mathbf{N}}_e^T d\Gamma, & a_e &= \int_{\Gamma_{ce}} \frac{h u_\infty^2}{2} d\Gamma \end{aligned} \quad (34)$$

Next, to enforce inter-element continuity on the common element boundary, the unknown vector  $\mathbf{c}_e$  should be expressed in terms of nodal DOF  $\mathbf{d}_e$ . The minimization of the functional  $\Pi_e$  with respect to  $\mathbf{c}_e$  and  $\mathbf{d}_e$ , respectively, yields

$$\begin{aligned} \frac{\partial \Pi_e}{\partial \mathbf{c}_e^T} &= -\mathbf{H}_e \mathbf{c}_e + \mathbf{G}_e \mathbf{d}_e = \mathbf{0} \\ \frac{\partial \Pi_e}{\partial \mathbf{d}_e^T} &= \mathbf{G}_e^T \mathbf{c}_e - \mathbf{g}_e - \mathbf{F}_e \mathbf{d}_e + \mathbf{f}_e = \mathbf{0} \end{aligned} \quad (35)$$

from which the optional relationship between  $\mathbf{c}_e$  and  $\mathbf{d}_e$ , and the stiffness equation can be produced:

$$\mathbf{c}_e = \mathbf{H}_e^{-1} \mathbf{G}_e \mathbf{d}_e \text{ and } \mathbf{K}_e \mathbf{d}_e = \mathbf{g}_e - \mathbf{f}_e \quad (36)$$

where  $\mathbf{K}_e = \mathbf{G}_e^T \mathbf{H}_e^{-1} \mathbf{G}_e - \mathbf{F}_e$  stands for the generalized element stiffness matrix.

### 3.5. Recovery of Generalized Rigid-body Motion

Considering the physical definition of the fundamental solution, it's necessary to recover the missing generalized rigid-body motion modes from above results.

Following the method presented in Ref.[20], the missing generalized rigid-body motion can be recovered by writing the internal potential field of a particular element  $e$  as

$$u_e = N_e c_e + c_0 \tag{37}$$

where the undetermined generalized rigid-body motion parameter  $c_0$  can be calculated using the least square matching of  $u_e$  and  $\tilde{u}_e$  at element nodes:

$$\sum_{i=1}^n (N_e c_e + c_0 - \tilde{u}_e)^2 \Big|_{\text{node } i} = \min \tag{38}$$

which finally gives

$$c_0 = \frac{1}{n} \sum_{i=1}^n \Delta u_{ei} \tag{39}$$

in which  $\Delta u_{ei} = (\tilde{u}_e - N_e c_e) \Big|_{\text{node } i}$  and  $n$  is the number of element nodes.

Once the nodal field is determined by solving the final stiffness equation, the coefficient vector  $c_e$  can be evaluated from Eq.(36), and then  $c_0$  is evaluated from Eq.(39). Finally, the potential field  $u$  at any internal point in an element can be obtained by means of Eq.(37).

## IV. NUMERICAL ASSESSMENTS

In order to evaluate the performance of the proposed approach, here we consider five typical examples for steady-state heat transfer in 2D functionally graded material and the results are compared with those from analytical and numerical methods. These examples cover the cases of a square of isotropic functional graded (FG) plate (Example 1 with exponential quadratic and trigonometric gradation), anisotropic FG plate whose thermal conductivities may vary in one direction (Example 2) or in two directions (Example 3), a FG annulus sector (Example 4), and a FGM bar with complicated geometry (Example 5).

The accuracy of the calculation results can be estimated by the average relative error on a variable  $f$ , which is defined as

$$\text{Arerr}(f(X)) = \sqrt{\frac{\sum_{i=1}^N (f^{(\text{num})}(X) - f^{(\text{an})}(X))_i^2}{\sum_{i=1}^N (f^{(\text{an})}(X))_i^2}} \tag{40}$$

where  $f^{(\text{num})}$  and  $f^{(\text{an})}$  are the numerical and exact result of the field variable.

### Example 1 A square of isotropic FG plate

Assume that the plate is isotropic and the thermal conductivity graded along the  $X_2$ -direction. Three graded types of FGM are considered in this example (exponential, quadratic and trigonometric). The side-length of the plate is  $a = 0.04$  m. The square FG plate with boundary conditions is shown in Fig.5. In the calculation,  $\beta$  is the graded parameter and material constant  $k_0 = 17$  W/m/°C are used. Only one 16-node quadrilateral element is used to model the solution domain (see Fig.6(a)).

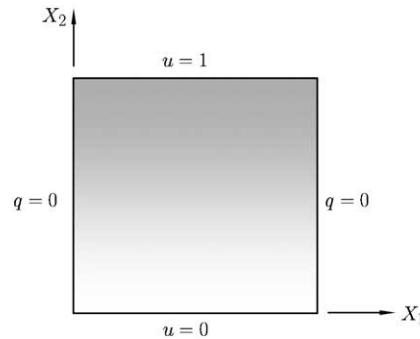


Fig. 5 Square FG plate and boundary condition in example 1.

#### (1) Exponential material gradation

The thermal conductivity follows the exponential law  $k = k_0 e^{2\beta X_2}$ . The calculation is conducted for different values of graded parameter  $\beta = 10, 25, 50$  m<sup>-1</sup>. The obtained numerical results are compared

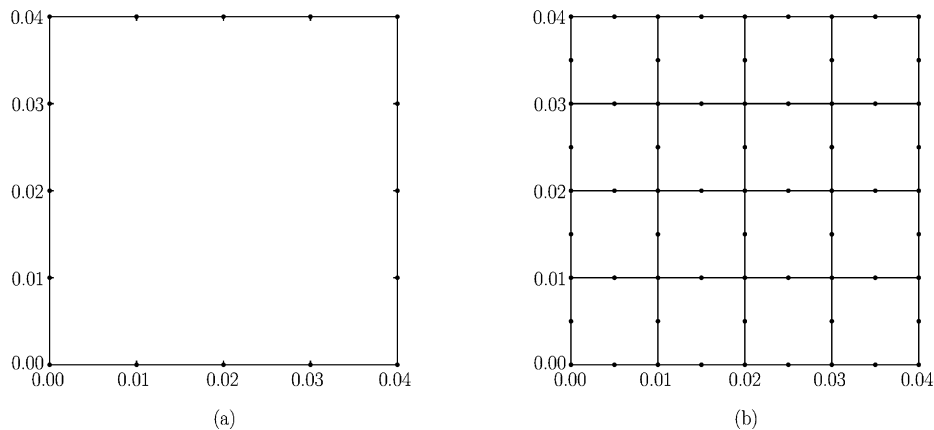


Fig. 6. (a) The mesh in proposed HFS-FEM, and (b) The mesh in the stepwise constant FEM.

with the following analytical solution<sup>[9,13]</sup>:

$$u = \frac{e^{-2\beta X_2} - 1}{e^{-2\beta a} - 1} \left( \lim_{\beta \rightarrow 0} u = \frac{X_2}{a} \right) \tag{41}$$

To investigate the effect of location of source points generated from Eq.(13), the calculation is conducted using different values of  $\gamma$ . It can be seen from Fig.7 that the numerical accuracy becomes acceptable and stable when  $\gamma$  is greater than 1.5 and the results are worse when  $\gamma$  is smaller than 1. This is because the small value of  $\gamma$  makes the source points too close to the field points, which may cause singularity of fundamental solution. Figure 8 shows that larger  $\gamma$  leads to larger condition number of matrix  $\mathbf{H}$  due to the round-off error in floating point algorithm. So, we choose  $\gamma = 2.5$  in our following calculation. Figure 9 shows the temperature distribution along  $X_2$  direction which is the graded direction. With an increasing  $\beta$ , the thermal conductivity increases and a higher level of temperature is obtained at the same position. An excellent agreement between numerical and analytical results is obtained for different graded parameters. It should be mentioned that such accuracy is achieved by just using one element in our approach.

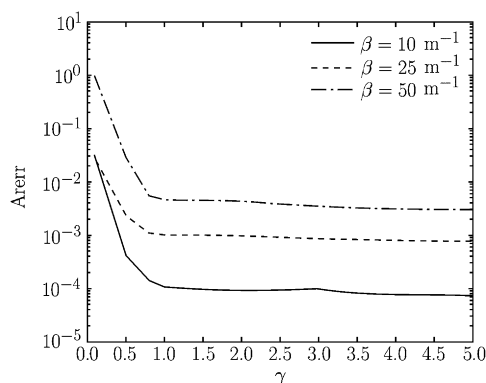


Fig. 7 Effect of various dimensionless parameter  $\gamma$  to numerical accuracy.

For the purpose of verification, the results are compared with those from conventional finite element simulation performed by the commercially available software ANSYS. With ANSYS, homogeneous elements are used. The material property of each element is taken at the centroid of each element and the material gradient is achieved by a highly refined mesh with 16 8-node quadrilateral elements (see Fig.6(b)). Table 1 compares the temperature of the interested points along the graded direction. It can be seen from Table 1 that the proposed method is more efficient than ANSYS because it can achieve more accurate results with much less elements. It should be mentioned that this example is also calculated using other meshless methods such as LBIE method<sup>[9]</sup> and virtual boundary collocation

Table 1. Comparison of temperature along  $X_2$  from HFS-FEM and ANSYS at  $\beta = 25 \text{ m}^{-1}$

$X_2$	0	0.005	0.01	0.015	0.02	0.025	0.03	0.035	0.04	Aerror
Exact	0	0.2558	0.4551	0.6102	0.7311	0.8252	0.8985	0.9555	1	
HFS-FEM	0	0.2556	0.4553	0.6102	0.7295	0.8252	0.8982	0.9556	1	$7.92 \times 10^{-4}$
ANSYS	0	0.2275	0.4551	0.5931	0.7311	0.8148	0.8984	0.94923	1	$1.65 \times 10^{-2}$

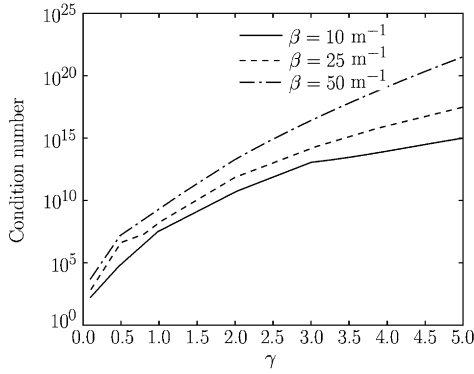


Fig. 8. Effect of various dimensionless parameter  $\gamma$  to condition number of matrix  $H$ .

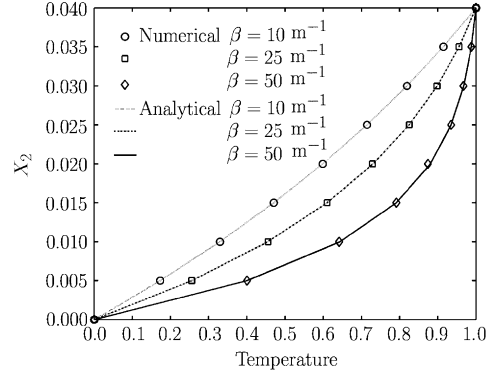


Fig. 9. Temperature distribution along the graded direction with various graded parameter  $\beta$ .

method (VBCM)<sup>[13]</sup>, in which equal 16 interior and boundary points are needed for approximation. In this paper, similar accuracy is obtained by the proposed method with only 16 boundary nodes and no interior nodes are involved.

(2) Quadratic material gradation

The thermal conductivity is assumed to follow the quadratic law  $k = k_0(1 + \beta X_2)^2$  ( $\beta = 5 \text{ m}^{-1}$  is adopted in the calculation). The fundamental solution used in Eq.(12) for quadratic FGM is derived based on the work [24] as

$$N(\mathbf{X}, \mathbf{X}_s) = \frac{1}{2\pi k_C(1 + \beta X_2)(1 + \beta X_{s2})} \ln(R) \tag{42}$$

And the analytical solution is

$$u = \frac{\sqrt{k_0}(1 + \beta L)X_2}{\sqrt{k}L} \tag{43}$$

It can be seen from Fig.10 that the numerical solution has an excellent agreement with the analytical solution.

To investigate the convergence of the proposed method, the calculation is also conducted by a series of meshes of  $N \times N$  elements. Table 2 displays the numerical accuracy with respect to different mesh densities. It can be seen from Table 2 that the relative error decreases along with refinement of the element meshes for both HFS-FEM and ANSYS, but in HFS-FEM, the numerical solution converges to the analytical solution more gradually and it can achieve high accuracy by only few elements.

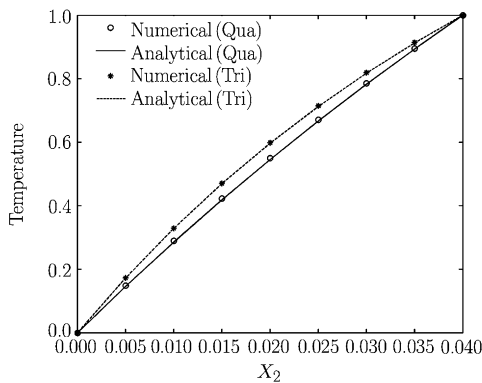


Fig. 10. Temperature distribution along the graded direction.

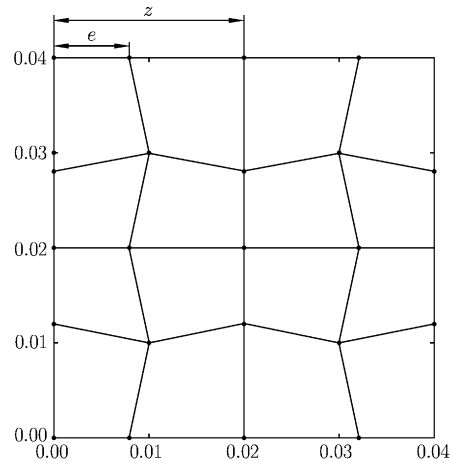


Fig. 11. Distorted mesh for example 1.

Table 2. Numerical results with mesh density

$N \times N$	$2 \times 2$	$4 \times 4$	$8 \times 8$
HFS-FEM	$9.1703 \times 10^{-4}$	$2.4725 \times 10^{-4}$	$6.2363 \times 10^{-5}$
ANSYS	$9.7192 \times 10^{-2}$	$2.6018 \times 10^{-2}$	$6.7950 \times 10^{-4}$

## (3) Trigonometric material gradation

The thermal conductivity follows the trigonometric law  $k = k_0[\cos(\beta X_2) + \sin(\beta X_2)]^2$  ( $\beta = 10 \text{ m}^{-1}$  is used in the calculation). The fundamental solution used in Eq.(12) for trigonometric FGM is derived based on the work [24] as

$$N(\mathbf{X}, \mathbf{X}_s) = \frac{1}{2\pi K_C [\cos(\beta X_2) + \sin(\beta X_2)][\cos(\beta X_{s2}) + \sin(\beta X_{s2})]} \ln(R) \quad (44)$$

The numerical results are compared with the analytical solution

$$u = \frac{\sqrt{k_0} [\cos(\beta \alpha) + 2 \sin(\beta \alpha)] \sin(\beta X_2)}{\sqrt{k} \sin(\beta X_2)} \quad (45)$$

Figure 10 shows that the numerical solution matches with the analytical solution very well.

Table 3. Comparison of temperature for distorted ( $e$  and  $z$  are shown in Fig.11 ) and undistorted  $4 \times 4$  element mesh along  $X_2$ 

$X_2$	Undistorted	Distorted for $e = 0.4z$	Distorted for $e = 0.3z$	Analytical
0.01	0.3071	0.3080	0.3102	0.3069
0.02	0.5681	0.5693	0.5712	0.5672
0.03	0.7976	0.8023	0.8034	0.7950

Table 3 shows the results of the study of sensitivity to mesh distortion. The results exhibit remarkable insensitivity to mesh distortion.

**Example 2** An anisotropic FG plate with varying thermal conductivities in  $X_2$ -direction

In this example, we consider a typical benchmark problem which is taken from Ref.[11]. In an anisotropic FGM square  $\Omega = \{X = (X_1, X_2) | 0 < X_1, X_2 < 1 \text{ m}\}$  subject to mixed boundary conditions as those in Example 1, the corresponding exact solution of the problem is

$$u(\mathbf{X}) = U_0 \frac{1 - \exp[-2(\beta_1 X_1 + \beta_2 X_2)]}{1 - \exp[-2(\beta_1 + \beta_2)]} \quad (46)$$

and the heat flux is

$$q(\mathbf{X}) = -2[n_1(\mathbf{X})(\tilde{K}_{11}\beta_1 + \tilde{K}_{12}\beta_2) + n_2(\mathbf{X})(\tilde{K}_{11}\beta_1 + \tilde{K}_{12}\beta_2)] \frac{U_0}{1 - \exp[-2(\beta_1 + \beta_2)]} \quad (47)$$

Specifically, the temperature  $u$  on two sides  $y = \pm 1 \text{ m}$  and the normal flux on the remaining two sides are specified. In the calculation,  $K_{11} = 3.0$ ,  $K_{12} = K_{21} = 0.0$  and  $K_{22} = 1.0 \text{ W/m}^\circ\text{C}$  are used, where  $U_0 = 100.0^\circ\text{C}$ ,  $\beta_1 = 0 \text{ m}^{-1}$ ,  $\beta_2 = 0.2 \text{ m}^{-1}$  (heat conductivity varies along direction  $X_2$  only).  $2 \times 2$  8-node quadrilateral elements are employed to model the solution domain.

Figure 12 illustrates the distribution of temperature in the FGM plate. The level of the largest percentage normalization is  $10^{-3}$ . The heat flux distribution in graded direction is shown in Fig.13(a)

and the corresponding normalized percentage error is plotted in Fig.13(b). It can be seen that the proposed model can achieve very high accuracy for both temperature field and heat flux field using a

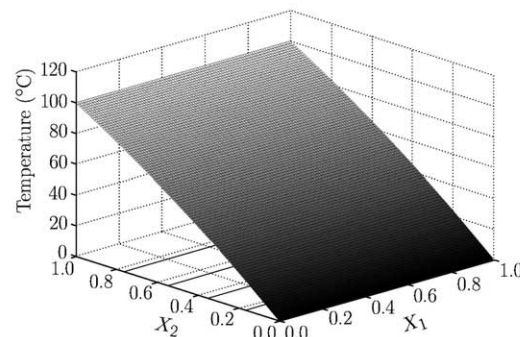


Fig. 12 Temperature distribution.

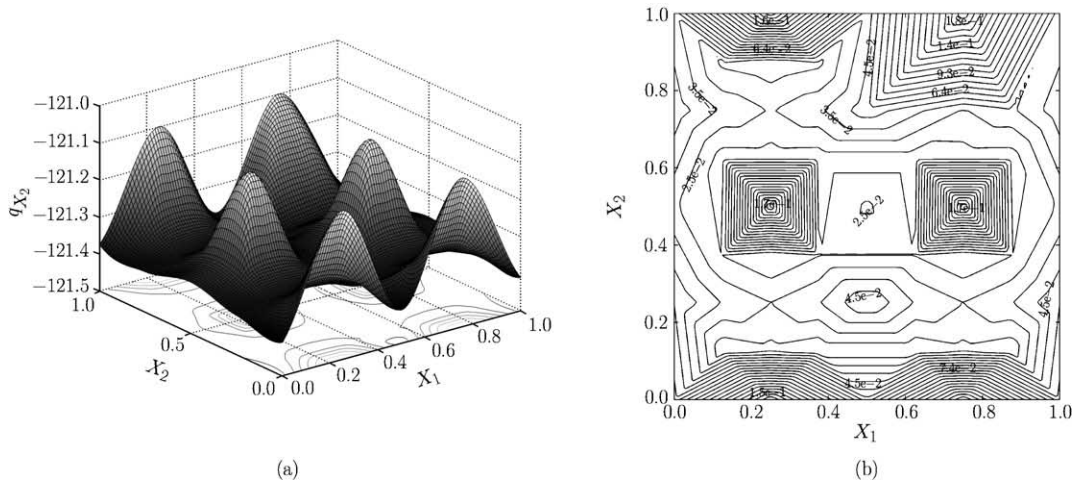


Fig. 13. (a) Distribution of heat flux  $q_{X_2}$  and (b) distribution of percentage normalized error of heat flux  $q_{X_2}$ .

small number of elements.

**Example 3** An anisotropic FG plate with varying thermal conductivities in both  $X_1$ - and  $X_2$ -directions

We consider the same solution domain, boundary condition and parameters, and the same number of elements as those in Example 2 are used for comparison purpose. But the heat conductivity varies along both direction  $X_1$  and  $X_2$ , with the graded constants  $\beta_1 = -0.5 \text{ m}^{-1}$ ,  $\beta_2 = 0.2 \text{ m}^{-1}$ .

Figure 14(a) shows the temperature distribution in the FGM plate and the corresponding numerical isothermal is presented in Fig.14(b). From Fig.14(c), it is apparent that it has already achieved a relatively high accuracy, although the error level is much higher than Example 2. This is because the material properties vary along two directions with different graded parameters ( $\beta_1 = -0.5 \text{ m}^{-1}$ ,  $\beta_2 = 0.2 \text{ m}^{-1}$ ) in this case. The higher accuracy can be achieved by increasing element mesh density. Figures 15 and 16 show heat flux in direction  $X_1$  and  $X_2$ , respectively. The largest error locates in the corner of the plate and its level is  $10^{-1}$ . The values of heat flux are much higher in  $X_2$  direction than those in  $X_1$  direction because of a larger graded parameter percentage normalized error distribution.

**Example 4** A FG annulus sector

In this example, a functionally annulus sector domain is considered. The boundary conditions of the problem are shown in Fig.17. The thermal conductivity graded along the  $X_1$ -direction is  $k = k_0 e^{2\beta X_1}$ , where  $k_0 = 17 \text{ W/m}^\circ\text{C}$  and  $\beta = 20 \text{ m}^{-1}$ . The inner and outer radii are assumed to be  $R_1 = 0.08 \text{ m}$  and  $R_2 = 0.1 \text{ m}$  in the calculation. 8-node quadrilateral elements are employed to model the solution domain and 4 elements are used to discretize along radial direction (see Fig.17). For comparison, the calculation is also done for homogeneous material ( $\beta = 0$ ) under the same condition. Figure 18 shows the isothermals for functionally graded material (FGM) and homogeneous material (HM). It can be seen that the isothermals for the homogeneous material are a set of concentric circular arcs, but offset for the FGM because of the graded material property.

**Example 5** FGM link bar

To further assess the performance of the proposed finite element model, consider a FGM link bar as is shown in Fig.18<sup>[2]</sup>. The bar is subject to mixed boundary conditions including temperature condition, heat flux condition and convection condition, as is shown in Fig.19. The thermal conductivity graded along the  $X_2$ -direction. The calculation is done for exponential, quadratic and trigonometric material gradation, respectively. In the following computation, following physical properties and temperatures are used:  $\beta = 10 \text{ m}^{-1}$ ,  $h = 1300 \text{ W}/(\text{m}^2 \cdot ^\circ\text{C})$ ,  $k_0 = 5 \text{ W}/(\text{m} \cdot ^\circ\text{C})$ ,  $T_0 = 300^\circ\text{C}$  and  $T_\infty = 1300^\circ\text{C}$ . The domain is discretized with 33 quadratic elements(see Fig.20(a)). For verification purpose, the results are compared with those from conventional finite element simulation performed by commercially available software ANSYS. With ANSYS, homogeneous elements with constant properties at the element level are used and the material gradient is achieved by a highly refined mesh with 135 quadratic elements (see Fig.20(b)). Contour plots of the temperature distribution obtained from proposed model are shown in Figs.21-23 and similar results can be obtained by using ANSYS. It should be mentioned that only few

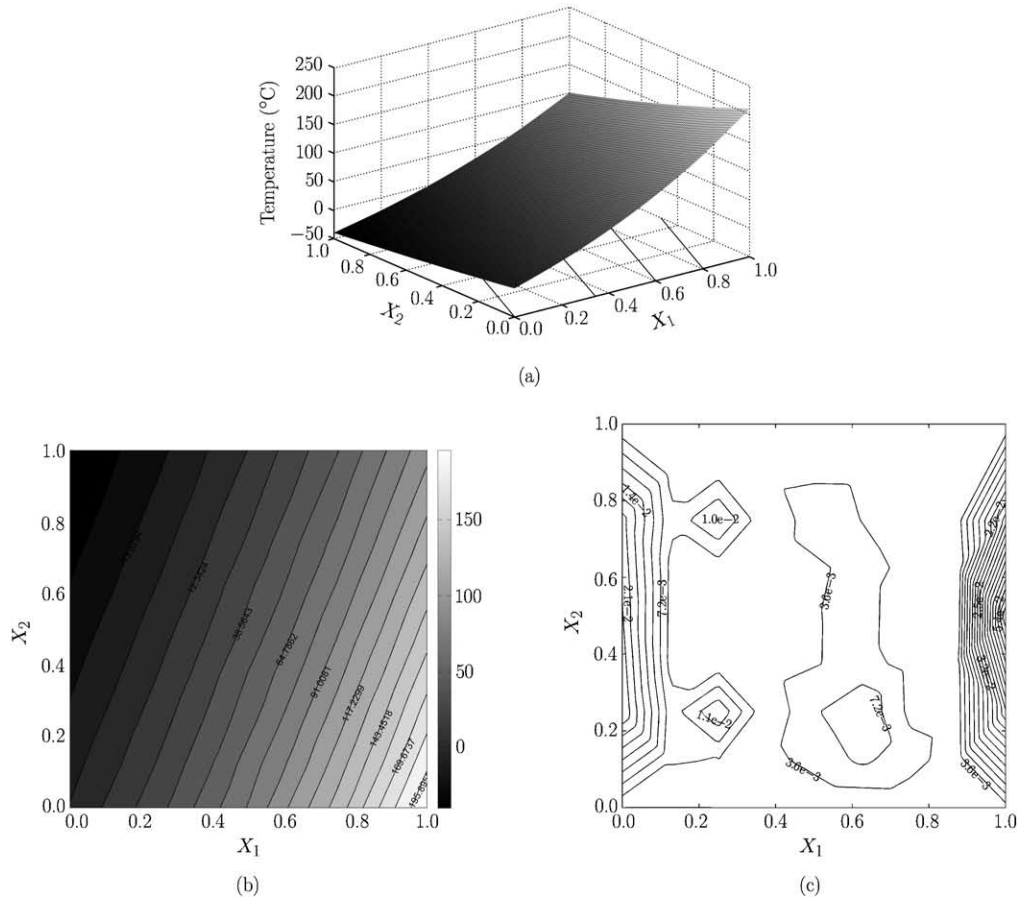


Fig. 14. (a) Temperature distribution, (b) numerical isotherms and (c) distribution of percentage normalized error of temperature.

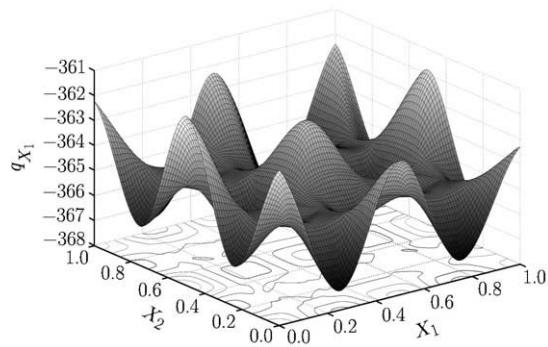


Fig. 15. Distribution of heat flux  $q_{X_1}$ .

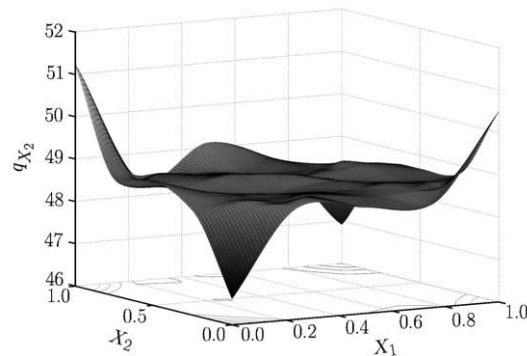


Fig. 16. Distribution of heat flux  $q_{X_2}$ .

elements are used in the proposed model and it contains some singular elements. The results exhibit remarkable insensitivity to the mesh distortion. For all those three cases, the peak temperature appears at the pointed corner of the bar. Table 4 compares the maximum temperature difference at those three kinds of FGM bars and homogeneous bar. It can be seen that the maximum temperature difference is lower in the FGMs than in the homogeneous material. Thus, the FGMs can lead to lower stress, which is an important advantage of FGMs. Moreover, exponential FGM shows best results with lowest temperature difference in this situation, quadratic FGM is better and trigonometric FGM is the worst one.

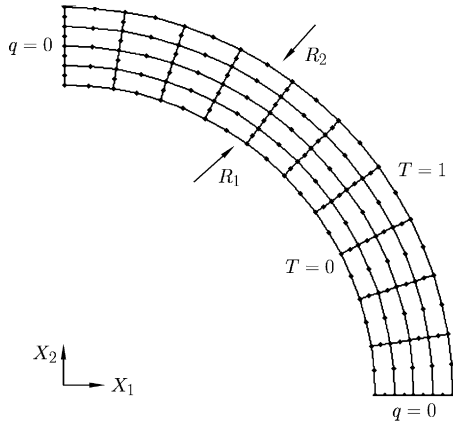


Fig. 17. Illustration of boundary conditions and mesh discretion for the quarter domain.

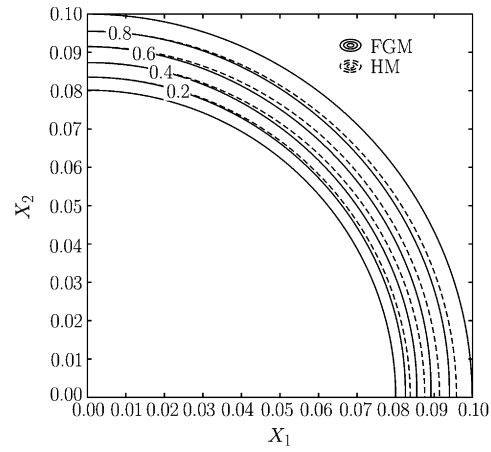


Fig. 18. Comparison of isothermal in FGM and HM.

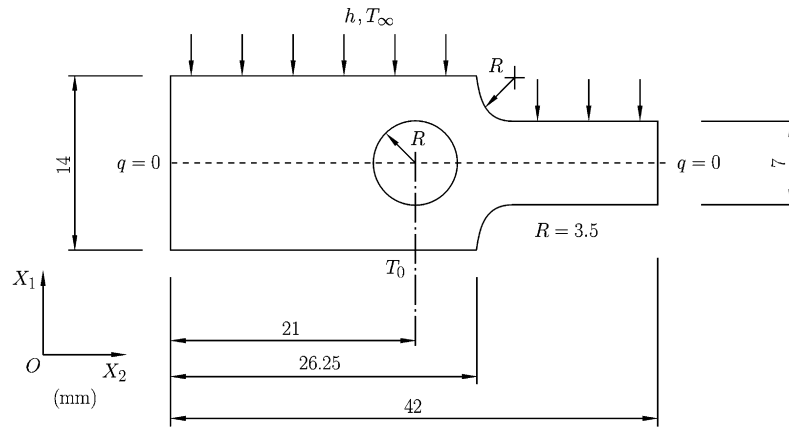


Fig. 19. Geometry and boundary conditions of FGM link bar.

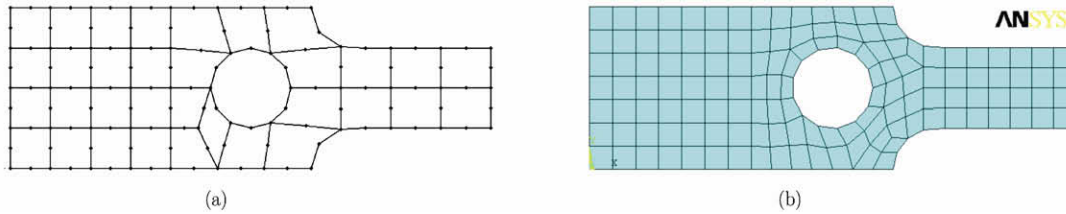


Fig. 20. (a) Computational mesh for the proposed HFS-FEM and (b) the conventional FEM.

Table 4. Comparison of maximum temperature difference at different FGM bars

Graded types	Exponential FGM	Quadratic FGM	Trigonometric FGM	Homogeneous material
Maximum temperature difference (°C)	927.8	960.2	989.0	1000.0

### V. CONCLUSIONS

In this paper, a new hybrid graded element model is developed for 2D steady-state heat conduction in functionally graded materials. In the model, the graded element which incorporate the material property gradient at the size of the element level, have been presented in internal element domain. A linear combination of the fundamental solution at points outside the element domain is used to

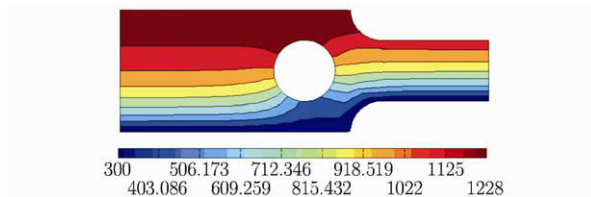


Fig. 21. Contour plots of the temperature distribution in exponential FGM bar.

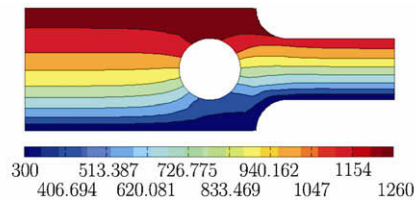


Fig. 22. Contour plots of the temperature distribution in quadratic FGM bar.

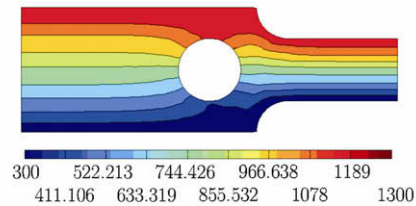


Fig. 23. Contour plots of the temperature distribution in trigonometric FGM bar.

approximate the field variable in the internal element domain and the boundary interpolation functions are used to construct the frame field. To assess the performance of the proposed model, several examples with continuous nonhomogeneous isotropic and anisotropic FGM are considered. The results show that the proposed method is an efficient approach, which has a high accuracy to simulate the heat behavior in FGM. In fact, it can approach the exact solution through continuous mesh refinement.

## References

- [1] Miyamoto, Y., Kaysner, W.A., Rabin, B.H., Kawasaki, A. and Ford, R.G., *Functionally Graded Materials: Design, Processing and Applications*. Dordrecht: Kluwer Academic Publishers, 1999.
- [2] Cao, L.L., Qin, Q.H. and Zhao, N., Hybrid graded element model for transient heat conduction in functionally graded materials. *Acta Mechanica Sinica*, 2012, 28(1): 128-139.
- [3] Chen, F.Y. and Jie, W.Q., Finite element design of MgO/Ni system functionally graded materials. *Journal of Materials Processing Technology*, 2007, 182(1-3): 181-184.
- [4] Paulino, G.H., Sutradhar, A. and Gray, L.J., Boundary element method for functionally graded materials. IABEM 2002, University of Texas, Austin.
- [5] Sutradhar, A. and Paulino, G.H., The simple boundary element method for transient heat conduction in functionally graded materials. *Computer Methods in Applied Mechanics and Engineering*, 2004, 193(42-44): 4511-4539.
- [6] Wen, J. and Khonsari, M.M., Transient heat conduction in rolling/sliding components by a dual reciprocity boundary element method. *International Journal of Heat and Mass Transfer*, 2009, 52(5-6): 1600-1607.
- [7] Ochiai, Y., Two-dimensional steady heat conduction in functionally gradient materials by triple-reciprocity boundary element method. *Engineering analysis with boundary elements*, 2004, 28(12): 1445-1453.
- [8] Wu, X.H. and Tao, W.Q., Meshless method based on the local weak-forms for steady-state heat conduction problems. *International Journal of Heat and Mass Transfer*, 2008, 51(11-12): 3103-3112.
- [9] Sladek, J., Sladek, V. and Zhang, Ch., Transient heat conduction analysis in functionally graded materials by the meshless local boundary integral equation method. *Computational Materials Science*, 2003, 28(3-4): 494-504.
- [10] Wang, H. and Qin, Q.H., Meshless approach for thermo-mechanical analysis of functionally graded materials. *Engineering analysis with boundary elements*, 2008, 32(9): 704-712.
- [11] Marin, L., Numerical solution of the Cauchy problem for steady-state heat transfer in two-dimensional functionally graded materials. *International Journal of Solids and Structures*, 2005, 42(15): 4338-4351.
- [12] Marin, L. and Lesnic, D., The method of fundamental solutions for nonlinear functionally graded materials. *International Journal of Solids and Structures*, 2007, 44(21): 6878-6890.
- [13] Wang, H., Qin, Q.H. and Kang, Y.L., A meshless model for transient heat conduction in functionally graded materials. *Computational mechanics*, 2006, 38(1): 51-60.
- [14] Wang, H., Qin, Q.H. and Kang, Y.L., A new meshless method for steady-state heat conduction problems in anisotropic and inhomogeneous media. *Archive of Applied Mechanics*, 2005, 74(8): 563-579.

- [15] Anlas,G., Santare,M.H. and Lambros,J., Numerical calculation of stress intensity factors in functionally graded materials. *International Journal of Fracture*, 2000, 104(2): 131-143.
- [16] Li,H., Lambros,J., Cheeseman,B.A. and Santare,M.H., Experimental investigation of the quasi-static fracture of functionally graded materials. *International Journal of Solids and Structures*, 2000, 37(27): 3715-3732.
- [17] Santare,M.H. and Lambros,J., Use of graded finite elements to model the behavior of nonhomogeneous materials. *Journal of Applied Mechanics*, 2000, 67(4): 819-822.
- [18] Gu,P., Dao,M. and Asaro,R.J., A simplified method for calculating the crack-tip field of functionally graded materials using the domain integral. *Journal of Applied Mechanics*, 1999, 66(1): 101-108.
- [19] Wang,H. and Qin,Q.H., Hybrid FEM with Fundamental Solutions as trial functions for Heat Conduction Simulation. *Acta Mechanica Solida Sinica*, 2009, 22(5): 487-498.
- [20] Qin,Q.H., The Trefftz Finite and Boundary Element Method. Southampton: WITpress, 2000.
- [21] Qin,Q.H. and Wang,H., Matlab and C Programming for Trefftz Finite Element Methods. CRC Press, 2008.
- [22] Wang,H. and Qin,Q.H., Boundary integral based graded element for elastic analysis of 2D functionally graded plates. *European Journal of Mechanics—A/Solids*, 2012, 33 : 12-23.
- [23] Cen,S., Fu,X.R. and Zhou,M.J., 8- and 12-node plane hybrid stress-function elements immune to severely distorted mesh containing elements with concave shapes. *Computer Methods in Applied Mechanics and Engineering*, 2011, 200(29-32): 2321-2336.
- [24] Berger,J.R., Martin,P.A., Mantič,V. and Gray,L.J., Fundamental solutions for steady-state heat transfer in an exponentially graded anisotropic material. *Journal of Applied Mathematics and Physics (ZAMP)*, 2005, 56(2): 293-303.
- [25] Gray,L.J., Kaplan,T., Richardson,J.D. and Paulino,G.H., Green's functions and boundary integral analysis for exponentially graded materials: heat conduction. *Journal of Applied Mechanics*, 2003, 70(4): 543-549.
- [26] Wang,H. and Qin,Q.H., Some problems with the method of fundamental solution using radial basis functions. *Acta Mechanica Solida Sinica*, 2007, 20(1): 21-29.
- [27] Wang,H. and Qin,Q.H., A meshless method for generalized linear or nonlinear Poisson-type problems. *Engineering analysis with boundary elements*, 2006, 30(6): 515-521.